Cerebral Cortex, September 2017;27: 4396–4410

doi: 10.1093/cercor/bhw242
Advance Access Publication Date: 1 September 2016
Original Article

ORIGINAL ARTICLE

Interaction of Intrinsic and Synaptic Currents Mediate Network Resonance Driven by Layer V Pyramidal Cells

Stephen L. Schmidt[1,2], Christopher R. Dorsett[1,3], Apoorva K. Iyengar[4], and Flavio Fröhlich[1,2,3,5,6,7]

[1]Department of Psychiatry, [2]Joint UNC-NCSU Department of Biomedical Engineering, [3]Neurobiology Curriculum, [4]Department of Biology, [5]Department of Cell Biology and Physiology, [6]Neuroscience Center, and [7]Department of Neurology, University of North Carolina at Chapel Hill, Chapel Hill, NC 27599, USA

Address correspondence to Flavio Fröhlich, Department of Psychiatry, University of North Carolina at Chapel Hill, 115 Mason Farm Road. NRB 4109F, Chapel Hill, NC 27599, USA. Email: flavio_frohlich@med.unc.edu

Note that a subset of the data included in this submission was previously presented in abstract form (SfN 2015 Chicago).

Abstract

Cortical oscillations modulate cellular excitability and facilitate neuronal communication and information processing. Layer 5 pyramidal cells (L5 PYs) drive low-frequency oscillations (<4 Hz) in neocortical networks in vivo. In vitro, individual L5 PYs exhibit subthreshold resonance in the theta band (4–8 Hz). This bandpass filtering of periodic input is mediated by h-current (I_h) and m-current (I_M) that selectively suppress low-frequency input. It has remained unclear how these intrinsic properties of cells contribute to the emergent, network oscillation dynamics. To begin to close this gap, we studied the link between cellular and network mechanisms of network resonance driven by L5 PYs. We performed multielectrode array recordings of network activity in slices of medial prefrontal cortex from the Thy1–ChR2–eYFP line and activated the network by temporally patterned optogenetic suprathreshold stimulation. Networks driven by stimulation of L5 PYs exhibited resonance in the theta band. We found that I_h and I_M play a role in resonant suprathreshold network response to depolarizing stimuli. The action of I_h in mediating resonance was dependent on synaptic transmission while that of I_M was not. These results demonstrate how synergistic interaction of synaptic and intrinsic ion channels contribute to the response of networks driven by L5 PYs.

Key words: h current, m current, resonance, multielectrode array, cortical slice

Introduction

Cortical oscillations are periodic fluctuations in excitability and represent a fundamental organizational principle of neuronal activity in cortex (Buzsáki 2006). Low-frequency cortical oscillations (<4 Hz) have been traditionally associated with sleep (Achermann and Borbely 1997; Steriade et al. 2001; Bazhenov et al. 2002) and deep anesthesia (Jameson and Sloan 2006). However, a broader role has recently emerged since pronounced slow rhythmic fluctuations in membrane voltage and local field potential have been also found in the awake, resting animal (Crochet and Petersen 2006; Gentet et al. 2010; Sellers et al. 2014). Functionally, low-frequency cortical oscillations may play a key role in memory consolidation and synaptic scaling (Marshall et al. 2006; Tononi and Cirelli 2014). Mechanistically, layer 5 pyramidal cells (L5 PYs) have been associated with the genesis of low-frequency oscillations in cortex, in particular in the slow (<1 Hz) and delta (1–4 Hz) frequency bands. L5 PYs initiate individual up states both in vivo (Luczak et al. 2007; Chauvette et al. 2010) and in vitro (Sanchez-Vives and McCormick 2000). Furthermore, low-frequency, square-wave optogenetic stimulation of L5 PYs generated cortical up and down states in vivo that closely resembled those that occur during spontaneous, endogenous slow oscillations (Beltramo et al. 2013).

At the cellular level, L5 PYs express hyperpolarization-activated cyclic nucleotide-gated (HCN) channels (Santoro et al. 2000; Lorincz et al. 2002; Ulrich 2002). These channels mediate the hyperpolarization-activated depolarizing current, I_h, which acts as a pace-maker current in both cortical and thalamic cells (Luthi and McCormick 1998). In particular, I_h is responsible for subthreshold resonance, typically in the theta band but also outside of this frequency range, in the absence of network interactions for hyperpolarized membrane voltages in both pyramidal cells (Hutcheon et al. 1996; Leung and Yu 1998; Hu et al. 2002) and other excitatory cell types (Haas and White 2002; Erchova et al. 2004; Fransen et al. 2004; Engel et al. 2008; Yoshida et al. 2011). However, the absence of HCN-mediated theta resonance for more depolarized membrane voltages (Hu et al. 2002) suggests that, in active networks, the role of I_h in generating rhythmic network activity may differ. Indeed, optogenetic stimulation in vivo confirmed a key role of I_h in suprathreshold theta resonance at the network level but surprisingly only for periodic stimulation of parvalbumin positive cells (presumed interneurons) and not stimulation of pyramidal cells, despite the presence of I_h in pyramidal cells (Stark et al. 2013). The number of HCN channels along the apical dendrite of L5 PYs increases exponentially with distance from the soma (Kole et al. 2006), implying a functional role of I_h in modulating synaptic integration in addition to somatic depolarization (Magee 2000; Zhuchkova et al. 2013; Cuntz et al. 2014). Conversely, non-inactivating potassium current (I_M) from Kv7 channels mediates theta band resonance at depolarized membrane voltages in cells in isolation (Hu et al. 2002). Despite similar findings of theta band resonance in vitro, the resonant frequency of cells arising from I_M and I_h is dependent on a complex set of parameters and can vary with experimental conditions (Rotstein and Nadim 2014; Rotstein 2015). Indeed aside from regulation of the resting potential and mediation of somatic theta resonance, both I_h and I_M play a large role in dendritic integration (for review see Magee 2000). It has thus remained unclear if and how HCN- and Kv7-mediated single cell dynamics translate to networks driven by excitation of L5 PYs and to what extent these dynamics interact with excitatory and inhibitory synaptic activity.

To answer this question, we combined multichannel electrophysiology in vitro with optogenetic excitation of L5 PYs (Arenkiel et al. 2007). We hypothesized that the interaction of synaptic (both excitatory and inhibitory) and cellular mechanisms plays a key role in network-wide suprathreshold frequency responses. To test this hypothesis, we applied frequency-sweep (chirp) stimulation to a large number of L5 PYs in acute cortical slices. Network activation of L5 PYs has been shown, for low-frequency stimulation, to produce naturalistic network-wide activation in vivo (Beltramo et al. 2013). We were able to isolate synaptic from cellular components of the network frequency response and discern the interactions which lead to the emergence of frequency tuning of cortical networks by combining multielectrode array recordings with the application of pharmacological agents. To account for differences in baseline excitability, we introduce a metric of relative activity based on the spiking activity across all stimulation frequencies. We utilize this metric to specifically examine network resonance. Using this measure, resonance can be observed as greater spiking response across the network for a small set of stimulation frequencies which are not the lowest or highest stimulation frequencies (which would indicate a possible low-pass or high-pass response respectively).

Materials and Methods

Solutions

All reagents were purchased from Fisher Scientific (Waltham, MA) with the exception of bicuculline and kynurenic acid (Sigma-Aldrich, St. Louis, MO) and ZD-7288 and XE-991 (Tocris Bioscience, Bristol, UK). Sucrose solution (in mM): 83.0 NaCl, 2.5 KCl, 0.5 $CaCl_2$, 3.3 $MgSO_4$, 1.0 NaH_2PO_4, 26.2 $NaHCO_3$, 22.0 dextrose anhydrous, and 72.0 sucrose. Incubation solution: 119.0 NaCl, 2.5 KCl, 1.0 NaH_2PO_4, 26.2 $NaHCO_3$, 22.0 glucose, 2.0 $MgSO_4$, and 2.0 $CaCl_2$. Control artificial cerebral spinal fluid (control aCSF): 119.0 NaCl, 4.5 KCl, 1 NaH_2PO_4, 26.2 $NaHCO_3$, 22.0 glucose, 1.0 $MgSO_4$, and 1.0 $CaCl_2$. Kynurenic acid and bicuculline aCSF (Kyn + Bic aCSF): control aCSF with 1 mM kynurenic acid and 10 μM bicuculline added. XE aCSF: control aCSF with 10 μM XE-991 added. Kynurenic acid and bicuculline with XE-991 aCSF (Kyn + Bic + XE aCSF): control aCSF with 1 mM kynurenic acid, 10 μM bicuculline, and 10 μM XE-991 added. ZD aCSF: control aCSF with 5 μM ZD-7288 added. Kynurenic acid and bicuculline with ZD-7288 aCSF (Kyn + Bic + ZD aCSF): control aCSF with 1 mM kynurenic acid, 10 μM bicuculline, and 5 μM ZD-7288 added.

Slice Preparation

All animal procedures were performed in compliance with the National Institutes of Health guide for the care and use of laboratory animals (NIH Publications No. 8023, revised 1978) and approved by the Institute of Animal Use and Care of the University of North Carolina at Chapel Hill. Juvenile mice (p15–30) were deeply anesthetized with Euthasol (0.5 mL/kg, Virbac, Fort Worth, TX). The mice were then decapitated and the brains quickly extracted and placed in ice cold sucrose solution. The 200 μm coronal slices of medial prefrontal cortex (mPFC, including infralimbic and prelimbic cortex) were cut using a Vibratome VT1000s (Leica Microsystems, Wetzlar, Germany) and allowed to recover for at least 1 h in incubation solution at 34°C. Details of this procedure have been previously described (Schmidt et al. 2013).

Wide Field Fluorescence Imaging

A p28 mouse was anaesthetized with Euthasol and then transcardially perfused with PBS followed by 4% paraformaldehyde in PBS. The 50 μm slices containing mPFC were cut using a CM 3050S (Leica Microsystems), mounted, stained with DAPI, and protected with coverslips. Images were acquired using an Eclipse 80i (Nikon Instruments, Tokyo, Japan) under 20× objective.

Patch Experimental Design

Slices were placed in the recording chamber and Kyn + Bic aCSF perfused at a rate of 1.2 mL/min at 36°C. MPFC was located under 4× objective and cells with ChR2/eYFP patched under 40× objective using a SliceScope (Scientifica, Uckfield, UK). Current clamp experiments were recorded in pClamp (Molecular Devices, Sunnyvale, CA) with a sampling rate of 5 kHz. Input and output were provided by a Digidata 1440A (Molecular Devices) and amplified by a MultiClamp 700B (Molecular Devices). Before each stimulation sweep, a brief hyperpolarizing test pulse of −150 pA was applied for 100 ms. The current characterization protocol consisted of 1 s long current injections between −500 and 900 pA (in steps of 50 pA). After the

current characterization, increasing frequency ZAP current injections were performed by injecting current I_{inj} = 10 pA * sin $\left(\frac{\pi}{5}t^{2.5}\right)$ for time t ranging from 0 to 30 s. Decreasing frequency ZAP current injections were made by decreasing t from 30 to 0 s. ZAP injections were performed in 5 sweeps in both directions at resting potential, with an injection of −100 pA, and with −200 pA injected current when possible.

Multielectrode Array Experimental Design

Multielectrode array (MEA) experiments were performed as in Schmidt et al. (2014). Briefly, slices were placed on a 6 × 10 perforated array of 30 μm electrodes (100 μm spacing) for an MEA2100 (MultiChannel Systems, Reutlingen, Germany) and were perfused with aCSF at a rate of 7 mL/min. Fifty-nine simultaneous multiunit (MU) traces were recorded in MC_Rack (MultiChannel Systems). An optical fiber coupled to a LED460 (Prizmatix, Givat Shmuel, Israel) was placed over the slice so that 0.5 mW optogenetic stimulation was applied to the entire slice. Groups of 20 trials of stimulation were applied, each trial consisted of optogenetic square-wave stimulation (50% duty cycle) of 0.25, 0.5, 1, 3, 5, 7, 9, 13, 17, 21, 25, 29 Hz for 3 s each (except 0.25 and 0.5 Hz stimuli which were applied for 8 and 4 s, respectively) in increasing or decreasing order. Increasing and decreasing trials were chosen in a random order. To account for the preferential response to the onset of stimulation, 50 s of 10 Hz stimulation was applied before the start of the first trial and during the 20 s between chirp stimuli. After the last trial, the perfusion was switched to a second type of aCSF based on the experiment. Twenty additional chirp stimuli were applied for 10 min after the switch of aCSF to allow the changes caused by the new aCSF to reach steady state. Fluorescence images of the slices on the MEA were captured using a Summit K2 (OptixCam, Roanoke, VA). EYFP within slices was excited and background light filtered using the SFA-Cyan (NightSea, Lexington, MA).

Data Analysis

All data were analyzed with custom-written Matlab scripts (The Mathworks, Natick, MA). The resting membrane voltage was calculated for each sweep before current injections by taking the median of membrane voltage occurring before the hyperpolarizing test pulse. The steady-state response to current injections (V_{steady}) was determined by taking the median value of the membrane voltage during the last 20 ms of the 1 s pulses minus the resting state V_m in the current characterization protocol. For hyperpolarizing pulse, V_{min} was calculated as the most negative voltage in response to a hyperpolarizing pulse minus the resting state voltage. The sag ratio was therefore calculated as V_{min}/V_{steady}.

For subthreshold ZAP current injections, any sweeps exhibiting deflections in V_m greater than 10 mV during the ZAP were excluded from analysis. Additionally, if more than 2 of the sweeps for an increasing or decreasing frequency ZAP experiment were excluded, then the experiment was excluded from group analysis. The resting membrane voltage was calculated for each sweep before ZAP current injections by taking the median of membrane voltage occurring before the hyperpolarizing test pulse. Voltage and current power spectra were calculated from 0.5 to 50 Hz using the Chronux toolbox function mtspectrumc() in Matlab (Mitra and Bokil 2008, chronux.org). A multitaper method was used in preference to FFT due to the nonstationary nature of ZAP stimuli. The voltage and current signal power spectra were converted to amplitude spectra and divided following Ohm's law to yield impedance spectra. The resonant frequency was determined as the frequency with the maximum impedance between 0.5 and 40 Hz. Q-value was calculated by dividing the amplitude of the impedance at the resonant frequency divided by that of the lowest frequency 0.5 Hz (Hutcheon et al. 1996).

The MU traces recorded by the MEA were high-pass filtered (300 Hz—fourth order Butterworth) and spikes were extracted where the voltage crossed −4 times the standard deviation for that MU trace (1 ms dead time). MU traces were included in subsequent analysis if the electrode was in mPFC and the average firing rate (FR) across the duration of the experiment was >0.5 spikes/s. Time courses were calculated (1 s bins) for each MU channel and z-scored by channel for the duration of the recording. z-Score was used to normalize the differences in FR dynamics across the MU in the slice. The mean of the z-scored data was plotted for each slice for purposes of visualizing the experiment only. Response to the conditioning stimulus for each trial was determined by the average FR of MU during the last 10 s of the conditioning stimulus before each trial. FR was calculated for each stimulation frequency as the total number of spikes divided by the duration of the stimulation for that frequency. The percentage of the total relative activity was calculated for each stimulation frequency i using the following equation:

$$\text{Relative Activity} = 100\% * \frac{FR_i}{\sum_{j=1}^{\#\text{ of stimulation frequncies}} FR_j} \quad (1)$$

FR, rather than spike count, was used to account for the differences in stimulation duration. By subsequent normalization for the total FR of all stimulation frequencies, this metric compensated for the change in baseline excitability caused by pharmacological changes to the aCSF. The resonant frequency was determined by the stimulation frequency with the largest relative activity (across all layers) for each chirp stimulus. A two-way ANOVA with factors of trial frequency direction and trial epoch (aCSF type) was used to determine statistical differences in resonant frequency.

To locate MU within L5 on the multielectrode array, the electrodes were superimposed over the fluorescence image of the slice on the array. Only electrodes within mPFC were included for analysis. Activity from electrodes was placed into 1 of the 2 groups for analysis: MU within L5 (identified by the region of eYFP) and those outside of L5 (above or below the region of eYFP).

Reported data in the text and error bars represent the 2.5–97.5% (2-sided 95%) confidence interval of the median using a 100-iteration bootstrapping algorithm. Statistical significance of the relative response to optogenetic stimuli in the MEA experiments was determined by a four-way ANOVA with factors frequency, chirp direction (increasing or decreasing frequency sweep), trial epoch, and MU layer. Differences between MEA experiment types were determined by a three-way ANOVA with factors frequency, chirp frequency direction, and experiment type. Tukey's HSD criterion was used for correction of multiple comparisons where appropriate.

Results

Networks Activated by L5 PYs Exhibited Resonance

We first probed the suprathreshold frequency response in MEA experiments by utilizing a preparation of acute cortical slices of mPFC from the Thy1–ChR2 mouse line which expressed

channelrhodopsin (ChR2) and eYFP in L5 PYs (Fig. 1A, left: eYFP image showing localization of ChR2 in L5 PYs, right: inset displaying apical dendrites). Slices were placed on an MEA and activity from many layers of mPFC was simultaneously recorded (Fig. 1B, green indicates ChR2 expression, electrodes are superimposed in cyan). We applied 20 chirps of increasing or decreasing frequency (10 each) square-wave (50% duty cycle) optogenetic stimulation in control aCSF (Fig. 1C, example chirps). We observed a strong initial response to the optogenetic stimulation which quickly faded to a steady-state response (Fig. 1D, red arrow). To suppress this transient response during chirp stimuli, we applied a conditioning stimulus for 50 s before the first trial and 20 s between subsequent trials. Ten minutes after completing the first epoch of 20 trials a second epoch of stimulation was applied (Fig. 1D, ~ 1300 s). During the second epoch the average FR response to the conditioning stimulus was increased (median [95% confidence interval], L5: 3.85 [3.28–4.53] spikes/s in the first epoch of stimulation and 3.81 [3.60–4.65] spikes/s in the second epoch of stimulation, other layers: 1.88 [1.65–2.05] spikes/s in the first epoch of stimulation and 2.33 [2.22–2.73] spikes/s in the second epoch of stimulation, $n = 180$ trials, $P = 0.132$ and $<10^{-3}$, respectively, Wilcoxon signed rank). The relative activity by frequency was different between optogenetic sweeps of increasing and decreasing frequencies ($P < 10^{-3}$, four-way ANOVA, see Methods section). However, the relative activity was not different between epochs for both MU in L5 and MU in other layers (with the exception of L5 MU at 5 and 7 Hz for increasing frequency stimuli, $P = 0.030$ and 0.027 and 0.25 Hz for decreasing frequency chirps, $P = 0.047$, there were no significant differences for MU outside L5, $n = 90$ trials, Supplementary Tables 1–4, Fig. 1E for MU within L5 and Fig. 1F for MU outside of L5). We therefore examined increasing and decreasing frequency sweeps separately, but have demonstrated that our stimulation paradigm did not evoke a different response due to the time elapsed during the experiment. We next asked if the largest relative activity was evoked by the lowest stimulation frequency (a low-pass filter response) or if larger relative activities were evoked by a few, slightly higher frequencies of stimulation (resonant response). We observed a peak in the frequency response of the relative activity across the network in the delta to low-theta range (resonant frequency for increasing frequency chirps: 3.01 [2.68–3.57] Hz for first control and 2.35 [2.07–2.56] Hz for second control; resonant frequency for decreasing frequency chirps: 5.00 [4.57–5.50] Hz for first control and 4.43 [3.61–5.58] Hz for second control; $n = 90$ trials for each condition; $P = 0.251$ and 0.502, respectively ANOVA). Due to the

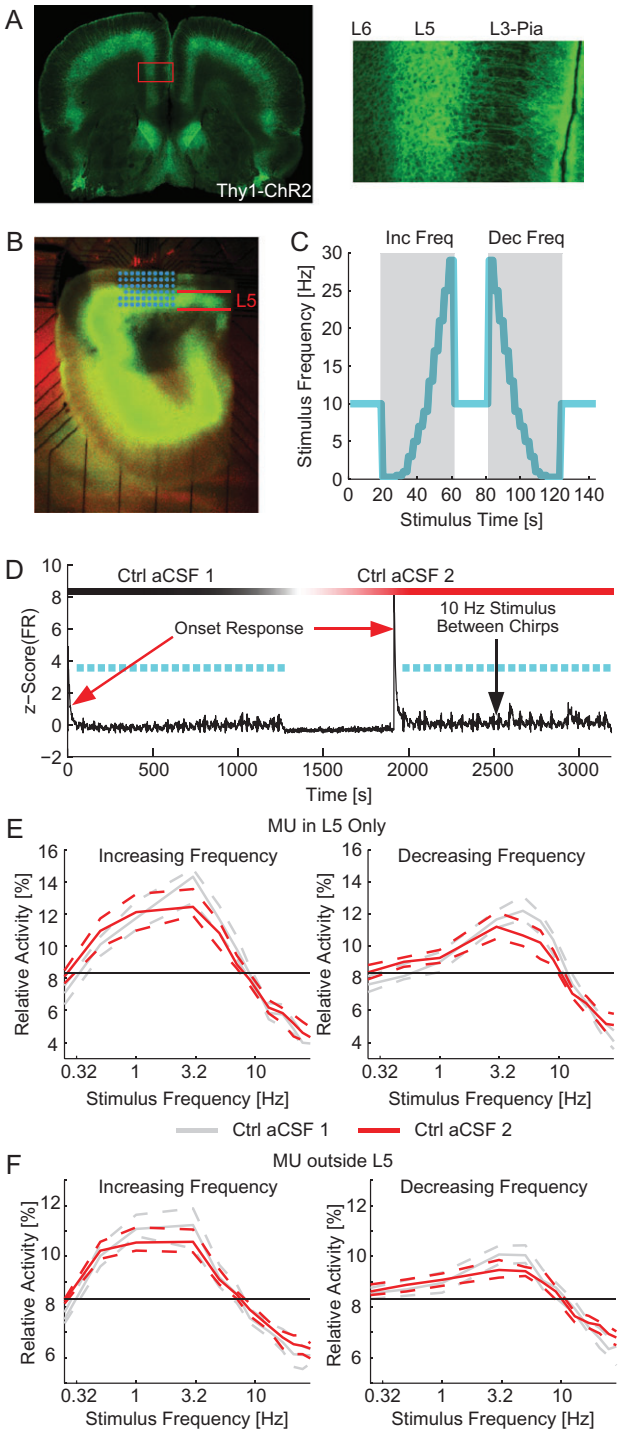

Figure 1. Network resonance by optogenetic activation of L5 PYs. (*A*) Fluorescence images of a coronal section containing mPFC. Left: eYFP expression throughout a coronal section, all neocortical regions express eYFP in L5. Right: Zoom-in of mPFC displaying eYFP in cell bodies and dendrites of cells originating in L5. (*B*) Fluorescence image of an experimental slice on the MEA. L5 indicated in red. MEA electrodes superimposed in cyan. (*C*) Frequency of optogenetic stimulation (cyan) for 2 sample trials denoted with gray background. A 10 Hz conditioning stimulus is applied for 20 s between trials. Trials consisted of chirp stimuli ranging from 0.25 to 29 Hz applied in either increasing (left) or decreasing (right) order. (*D*) The mean z-scored firing rate for all MU during an experiment (black). Frequency sweeps are indicated in cyan. After the completion of the first epoch of stimulation (~1300 s), the perfusion was switched to another container of control aCSF. A second epoch of stimulation was applied 10 min after switching the aCSF (~1900 s here). The red arrows illustrate the strong onset response to the start of stimulation epochs. Black arrow indicates the response during the 20 s of 10 Hz stimulus between chirps. (*E*) The relative activity for each frequency of stimulation for increasing (left) and decreasing (right) frequency chirp stimuli for MU in L5. The response during the first epoch of stimulation is in gray. The response of the second epoch of stimulation is in red. The black line indicates chance level of activity. In both cases, the network exhibited a resonant frequency in the high delta to low theta range. (*F*) The relative activity for each frequency of stimulation for increasing (left) and decreasing (right) frequency chirp stimuli for MU outside of L5 (including L1, L2/3, and L6). The response during the first epoch of stimulation is in gray. The response of the second epoch of stimulation is in red. In both cases, the network exhibited a resonant frequency in the high delta to low theta range. Inc Freq, increasing frequency chirps; Dec Freq, decreasing frequency chirps; Ctrl aCSF, control aCSF. Dashed lines indicate the 95% confidence interval of the median.

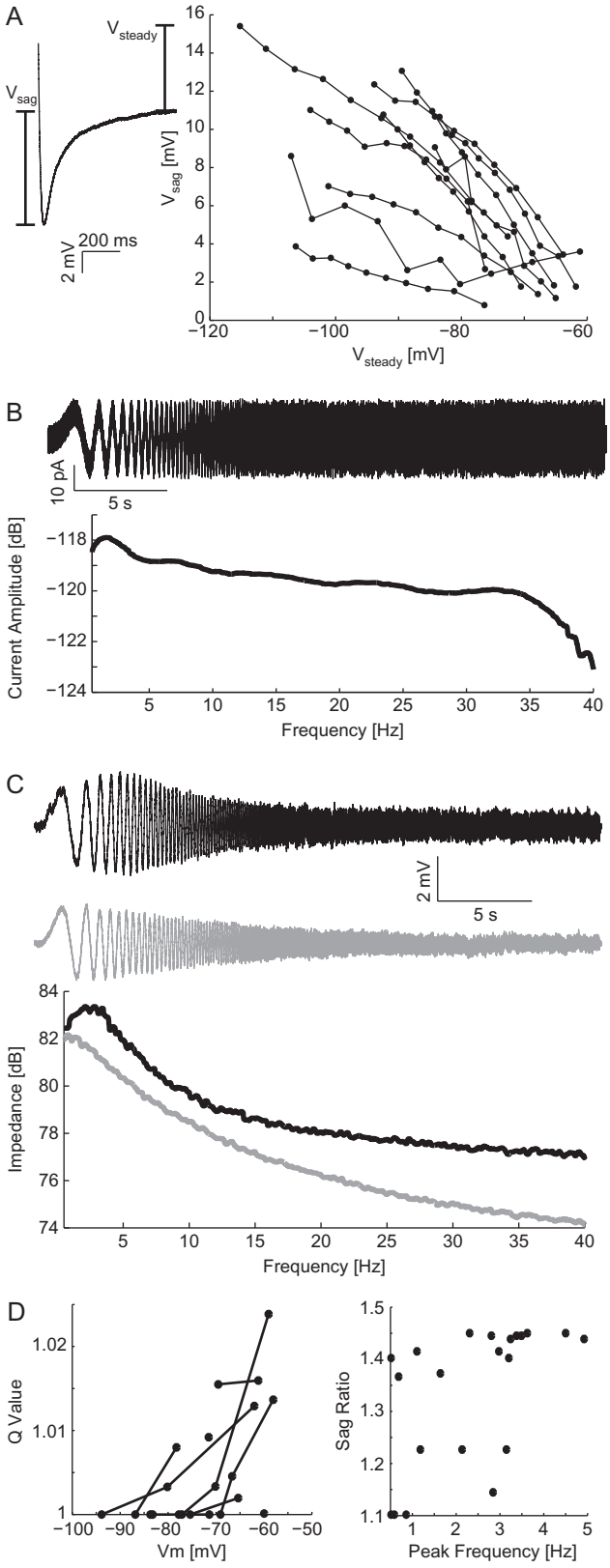

Figure 2. Patch recordings of eYFP/ChR2-labeled cells. (*A*) V_{sag}, as a measurement of I_h, in response to hyperpolarizing current injections versus the V_{steady}. The 2 values were highly correlated for all cells. (*B*) ZAP current injections in time (top) and frequency (bottom) domains. (*C*) Example recorded V_m (top) and calculated impedance spectra (bottom) for a cell with a resonant peak (black) and one with a preference for low frequency (gray) in response to ZAP stimulation. (*D*) *Left*: Q-value versus V_m for all ZAP stimuli. *Right*: Sag ratio versus the peak frequency for all cells. The peak frequency was correlated with sag ratio indicating that the resonant frequency was partially determined by the magnitude of I_h.

high-delta to the low-theta resonant frequency, we hypothesized that intrinsic cellular resonance played a major role in the network response. We specifically targeted resonance mediated through I_M and I_h. Due to the previous work on the effect of I_h on network oscillations (Rotstein et al. 2005; Giocomo and Hasselmo 2009; Stark et al. 2013), we hypothesized that such currents play a critical role in the resonance phenomenon observed here at the network scale.

A subset of eYFP-Labeled L5 PYs Exhibited Subthreshold Resonance

We next sought to confirm subthreshold resonance in eYFP-labeled L5 PYs in the mPFC of the Thy1–ChR2 mouse line. These cells are activated by the application of blue light and, therefore, drive the response to optogenetic chirp experiments. To examine the subthreshold resonance of these cells, we performed current clamp recordings at the somata of eYFP-labeled L5 PYs with synaptic transmission suppressed (Kyn + Bic aCSF, aCSF with the addition of 10 μM bicuculline to suppress $GABA_A$ and 1 mM kynurenic acid to suppress AMPA and NMDA transmission). We first observed the strength of I_h by applying hyperpolarizing current pulses and measuring V_{sag} (Fig. 2*A*). The amplitude of V_{sag} varied between cells but was inversely correlated with V_{steady} for each cell ($r = -0.697$ Spearman's correlation for least correlated cell, $P < 0.05$, $n = 10$ cells). We next performed subthreshold frequency sweep current injections (ZAP stimuli) of both increasing and decreasing frequencies (Fig. 2*B*, top: increasing frequency ZAP current in the time domain and bottom: ZAP current in the frequency domain). As in Hu et al. (2002), the resonant frequency in response to ZAP stimuli did not differ between increasing and decreasing frequency stimuli ($P = 0.408$, $n = 19$ pairs of ZAP experiments). We observed both low-pass and resonant frequency responses which varied between cells as previously observed in mPFC in Dembrow et al. (2010; Fig. 2*C*). We quantified deviation from a low-pass response by calculating Q-value (Fig. 2*D* left). In this metric, a value of 1 means that the amplitude at the resonant frequency was the same as that of the lowest frequency, indicating a low-pass filter-like response. Finally, we examined the correlation between sag ratio (see Methods section) and resonant frequency (Fig. 2*D*, right). The sag ratio of the cells and therefore activation of I_h was correlated to the resonant frequency ($r = 0.679$ Spearman's correlation, $P < 10^{-3}$, median V_m: −71.4 [−77.8 to 66.6] mV). We interpret these results to indicate that population of eYFP-labeled cells consisted of both cells which do exhibit and cells which do not exhibit subthreshold resonance.

Resonant Peak Shifted to Lower Frequencies with Synaptic Transmission Suppressed

In addition to cellular components, synaptic transmission may also contribute to the resonant response of networks. To test this for our experimental paradigm, we performed MEA experiments to examine the effect of suppressing synaptic transmission with kynurenic acid (to suppress AMPA and NMDA transmission) and bicuculline (to suppress $GABA_A$ transmission). If the effect of suppressing synaptic transmission was

simply a reduction in FR, then we would expect to see the same relative activity as in control. However, if the resonant profile is dependent on synaptic transmission, then the distribution of the relative activity would be different from control. To test for this effect, slices were given 20 optogenetic chirp stimuli (square-wave with 50% duty cycle) in control aCSF followed by 20 stimuli in Kyn + Bic aCSF (Fig. 3A, an example time course of the experiments). The response to the conditioning stimulus was decreased by suppressing synaptic transmission (MU inside L5: 8.66 [7.51–9.64] spikes/s in control aCSF and 3.14 [2.97–3.64] spikes/s in Kyn + Bic aCSF, MU outside of L5: 2.47 [2.35–2.60] spikes/s in control aCSF and 1.73 [1.62–1.87] spikes/s in Kyn + Bic aCSF, $P < 10^{-3}$ for both groups, Wilcoxon-ranked sum). We next examined the change in relative activity by frequency, a metric which accounted for changes in baseline FR (see Methods section). Within L5 the frequency response favored lower frequencies with synaptic transmission suppressed (Fig. 3B). This shift was accomplished by both increased response to low-frequency stimulation (0.25–1 Hz for increasing frequency chirps and 0.25–3 Hz for decreasing frequency chirps, four-way ANOVA, Supplementary Tables 1 & 2) and decreased response to stimulation in the middle of the frequency range (5–13 Hz for increasing frequency chirps and 7–13 Hz for decreasing frequency chirps). Outside of L5, there were few significant differences in frequency preference caused by the suppression of synaptic transmission (exceptions: increased response to 0.25 Hz and decreased response to 3–5 Hz, for increasing frequency chirps only, four-way ANOVA, Supplementary Tables 3 & 4, Fig. 3C). We observed a shift in the resonant frequency of the network due to the suppression of synaptic transmission in favor of low-frequency stimulation (increasing frequency sweeps: 3.09 [3.00–3.24] Hz for control aCSF and 1.94 [1.78–2.20] Hz for Kyn + Bic aCSF, decreasing frequency sweeps: 4.6 [4.29–4.93] Hz for control aCSF and 3.41 [2.98–4.17] Hz for Kyn + Bic aCSF, $P < 10^{-3}$ ANOVA, $n = 90$ trials for each condition). With synaptic transmission (AMPA, NMDA, and $GABA_A$) suppressed and therefore the number of post-synaptic potentials limited, the frequency response was shifted to favor lower frequency stimuli. These results support the hypothesis that synaptic transmission shapes the frequency response of neocortical networks activated by L5 PYs.

The Network Level Effect of I_M was Largely Independent of Synaptic Transmission

We probed the contribution of depolarization-activated current I_M by comparing the results of optogenetic stimulation during pharmacological blockade of KCNQ (Kv7.1, Kv7.2, and Kv7.3) channels to a preceding control epoch. To do so, we added 10 μM XE-991 to the aCSF (XE aCSF) used during the second epoch of stimulation (Fig. 4A, beginning at ~1900 s). As I_M returns depolarized cells to resting potential, we expected the blockade of I_M to increase the FR in response to the suprathreshold conditioning stimulus. Indeed, in response to the optogenetic conditioning stimulus in XE aCSF, the FR of L5 cells increased from 3.55 [2.98–4.14] spikes/s to 4.54 [3.88–4.91] spikes/s ($n = 180$ trials, $P = 0.036$ Wilcoxon-ranked sum); however, MU outside of L5 remained relatively constant (1.99 [1.90–2.09] spikes/s in control aCSF and 2.01 [1.92–2.10] spikes/s in XE aCSF, $P = 0.12$ Wilcoxon-ranked sum). We observed an expected decrease in the L5 response to stimuli in the middle of the frequency range (5–9 Hz for increasing frequency chirps and 9–21 Hz for decreasing frequency chirps, $P < 0.05$, four-way ANOVA, Supplementary Tables 1 and 2, Fig. 4B) as well as an increase in the L5 response to low-frequency stimuli (0.25–1 Hz for increasing frequency chirps and 0.25–3 Hz for decreasing frequency chirps). This result indicates that while the baseline FR activity has increased, the network preferentially responded to lower frequency stimuli when I_M was blocked. Importantly, we observed similar effects in MU outside of L5 (Fig. 4C, Supplementary Tables 3 and 4). Specifically, the response to stimulus in the middle frequencies of the sweep was decreased (5–9 Hz for increasing frequency chirps and 7–17 Hz for decreasing frequency chirps). The response to low-frequency stimuli was increased in MU outside of L5 as well (0.25–1 Hz for increasing frequency chirps and 0.25–3 Hz for decreasing frequency chirps). We next examined the change in the resonant frequency of the network. The blockade of I_M reduced the resonant frequency of the network (increasing frequency sweeps: 2.84 [2.68–2.96] Hz for control aCSF and 1.12 [0.994–1.31] Hz for XE aCSF, decreasing frequency sweeps: 5.07 [4.62–5.87] Hz for control aCSF and 2.92 [2.40–3.64] Hz for XE aCSF, $P < 10^{-3}$ ANOVA, $n = 90$ trials for each condition). These results indicate that the frequency response as a whole and, in particular, the resonant frequency of the network depended on I_M. Without I_M, the network preferentially responded to low-frequency stimulation.

We next performed experiments to assess the interaction of I_M with synaptic transmission. To do so, we used aCSF with synaptic blockers (Kyn + Bic aCSF) during the entire experiment. During the second epoch of stimulation we added XE-991 (Kyn + Bic + XE aCSF). The comparison of the 2 stimulation epochs allowed us to examine the effect of I_M while synaptic transmission was suppressed (Fig. 5A). With synaptic transmission suppressed, the addition of XE reduced the response to the conditioning stimulus (Kyn + Bic aCSF: 4.86 [4.50–5.08] Hz, XE + Kyn + Bic aCSF: 3.43 [3.18–3.80] Hz, $n = 160$ trials, $P < 10^{-3}$ Wilcoxon signed rank). Similar to experiments with XE alone, we observed a stronger relative activity for low frequencies (0.25–1 Hz) for MU in L5 as well as a decrease in response to higher frequency stimulation (5–21 Hz) for both increasing and decreasing frequency sweeps ($n = 80$ trials in each direction, $P < 10^{-3}$, four-way ANOVA, Supplementary Tables 1 and 2, Fig. 5B). MUs outside of L5 were similarly affected by the blockade of XE with a greater response to low-frequency stimulation (0.25–1 Hz for increasing frequency sweeps, 0.25 and 0.5 Hz for decreasing frequency sweeps) and a decreased response to middle frequency stimulation (3–9 Hz for increasing frequency sweeps, 5–13 Hz for decreasing frequency sweeps) compared with suppressed synaptic transmission alone ($n = 80$ sweeps for each condition, $P < 10^{-3}$ four-way ANOVA, Supplementary Tables 3 and 4, Fig. 5C). The resonant frequency was decreased across the network with the blockade of I_M (increasing frequency sweeps: 2.47 [2.23–2.68] Hz for Kyn + Bic aCSF and 0.713 [0.638–0.813] Hz for Kyn + Bic + XE aCSF, decreasing frequency sweeps: 4.23 [3.85–4.55] Hz for Kyn + Bic aCSF and 1.35 [1.25–1.53] Hz for Kyn + Bic + XE aCSF, $P < 10^{-3}$, $n = 80$ trials for each condition).

We compared the difference in frequency response caused by the blockade of I_M in control with that of the blockade of I_M with suppressed synaptic transmission by summing the absolute values difference in relative activity by frequency for all sweeps. The effect of the blockade of I_M was not different with synaptic transmission suppressed from the effect of the blockade of I_M with synaptic transmission intact (increasing frequency sweeps: 21.2 [19.3–22.9]% for XE aCSF and 19.35 [18.3–21.9]% Kyn + Bic + XE aCSF, decreasing frequency sweeps: 18.3 [17.1–18.9]% for XE aCSF and 20.4 [18.5–22.6]% for Kyn + Bic + XE

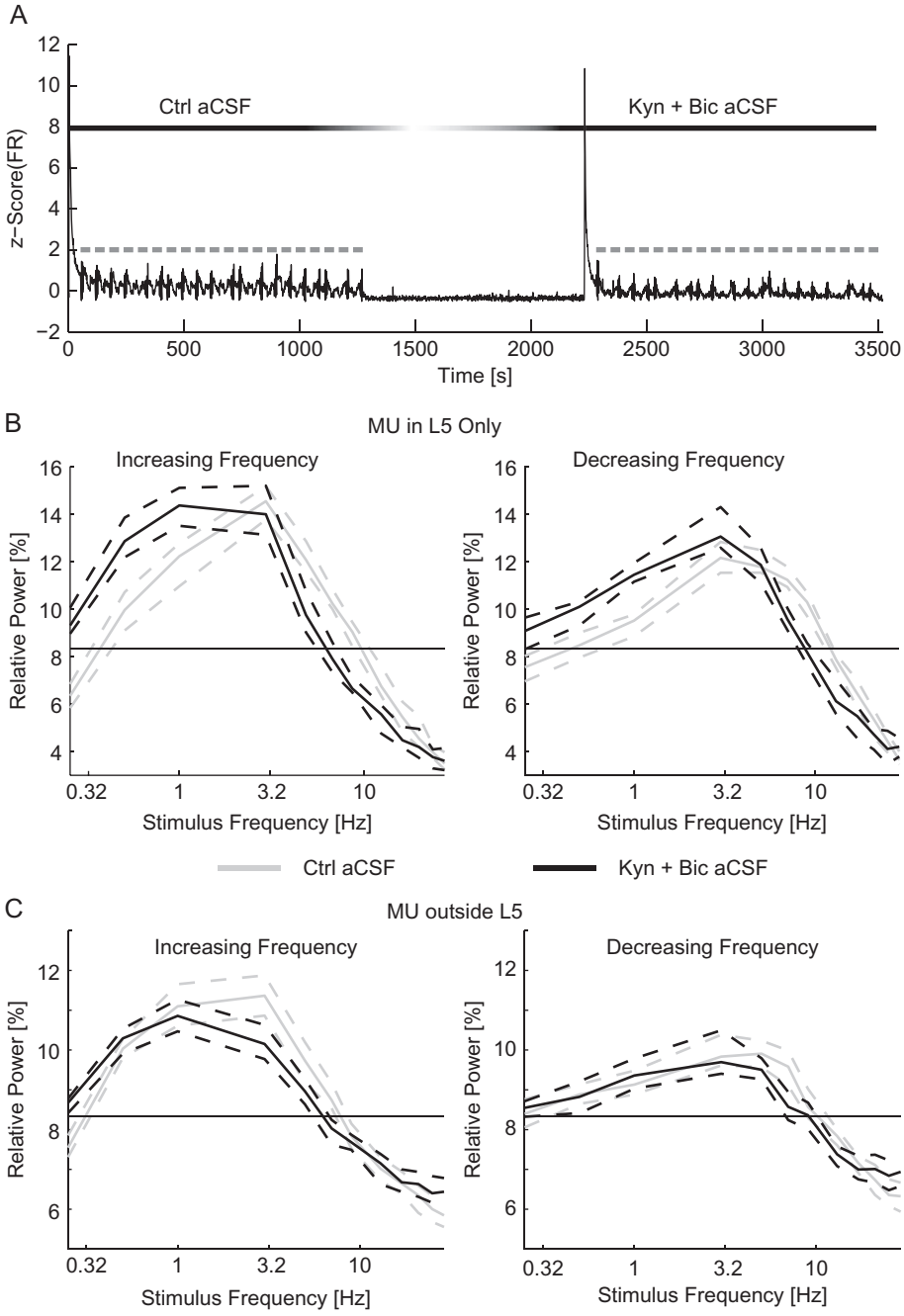

Figure 3. Suppression of synaptic transmission favors slower stimuli. (*A*) The z-scored time course of the MU firing rate (black) for the duration of the experiment. Optogenetic chirps are indicated in gray. After the first epoch of stimulation with control aCSF the perfusion was switched to Kyn + Bic aCSF. Ten minutes after the addition of synaptic blockers, a second epoch of stimulation was applied. The relative activity of MU recorded in L5 (*B*) and MU recorded outside of L5 (*C*) for increasing (left) and decreasing (right) frequency stimuli. For chirps in control aCSF (gray) and Kyn + Bic aCSF (black). The thin black line indicates chance activity levels. The addition of synaptic blockers caused a shift in the frequency response in favor of slow stimuli. Dashed lines indicate the 95% confidence interval of the median. Ctrl aCSF, control aCSF.

aCSF, $P = 0.988$ for increasing frequency sweeps and $P = 1.00$ for decreasing frequency sweeps ANOVA, $n = 90$ trials for XE aCSF and 80 trials for Kyn + Bic + XE aCSF in each direction frequency sweep). We interpret this result to indicate that the effect of I_M was largely independent of synaptic transmission. Taken together we observed that I_M affected the frequency response of networks but those effects were not dependent on synaptic transmission.

The Network Level Effect of I_h was Dependent on Synaptic Transmission

We next assessed the contribution of hyperpolarization-activated depolarizing current I_h on networks driven by L5 PYs. In order to isolate the contribution of I_h to the frequency response, we performed experiments using HCN channel antagonist ZD-7288. The effect of blocking I_h was determined by

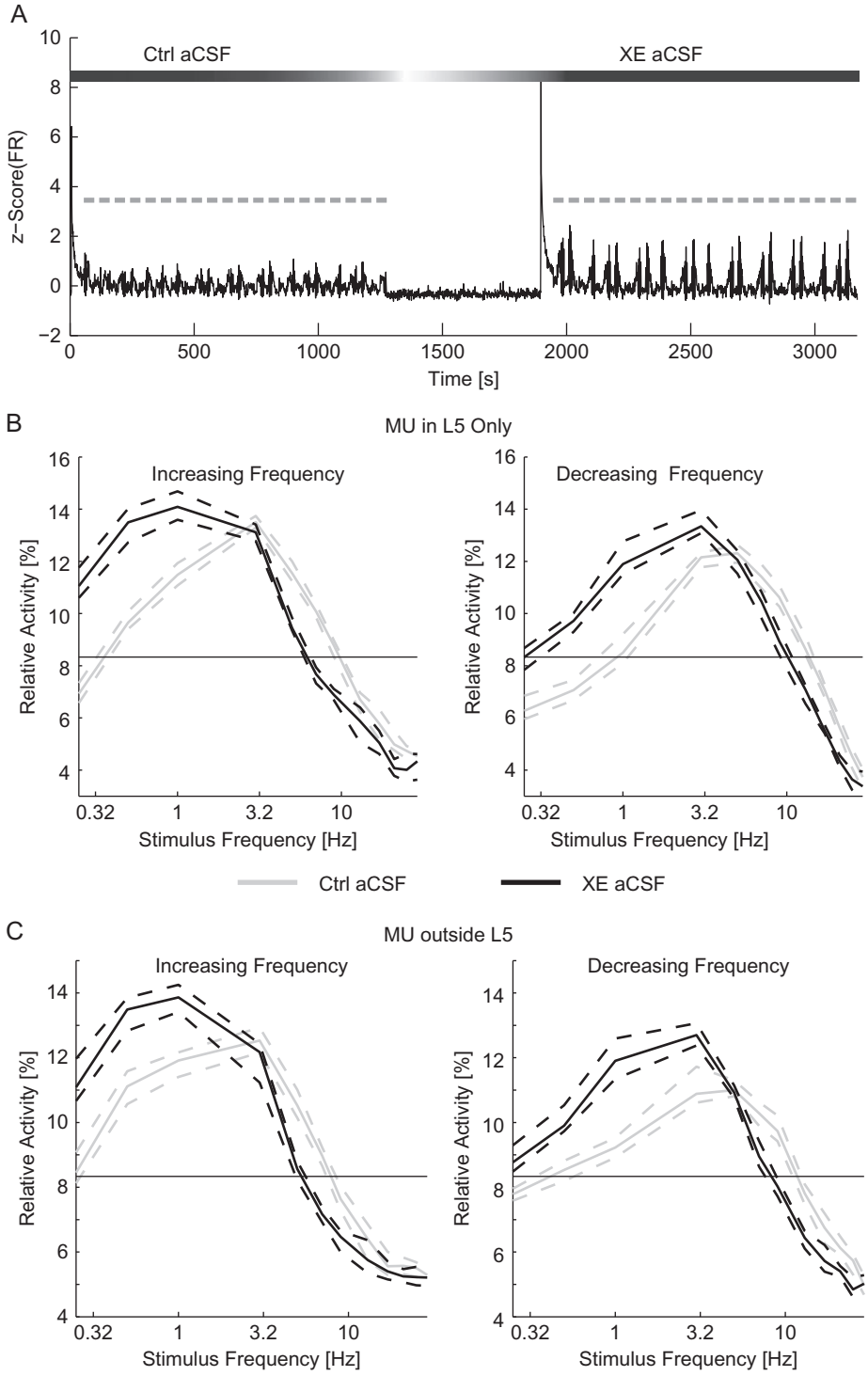

Figure 4. Addition of XE-991 reduced the resonant frequency of networks. (*A*) The z-scored time course of the MU firing rate (black). Chirp trials are indicated in gray. After the first epoch of stimulation, the perfusion was switched to XE aCSF. Ten minutes after the application of XE aCSF, a second epoch of stimulation was applied. (*B*) The relative activity for each frequency of stimulation for increasing (left) and decreasing (right) frequency chirps for MU recorded within L5. (*C*) The relative activity for MU recorded outside of L5 for increasing (left) and decreasing (right) frequency chirp stimuli. For (*B*) and (*C*), response to optogenetic chirps in control aCSF is in gray while the response to chirps delivered in XE aCSF is in black. The thin black line indicates chance activity levels. With XE-991 in the bath, the response to low-frequency stimuli was increased. Ctrl aCSF, control aCSF. Dashed lines indicate the 95% confidence interval of the median.

comparing trials of stimulation with ZD aCSF to trials of a previous within-slice control (Fig. 6A: example time course of an experiment). With I_h blocked, the response to the 10 Hz conditioning stimulus was reduced across the network (L5: 7.54 [6.2–7.94] spikes/s in control aCSF and 4.60 [4.26–5.05] spikes/s in ZD aCSF, other layers: 2.64 [2.35–2.92] spikes/s in control aCSF and 2.08 [1.93–2.20] spikes/s in ZD aCSF, n = 180 trials, $P < 10^{-3}$, Wilcoxon-ranked sum). Without I_h, the MU in L5 were less

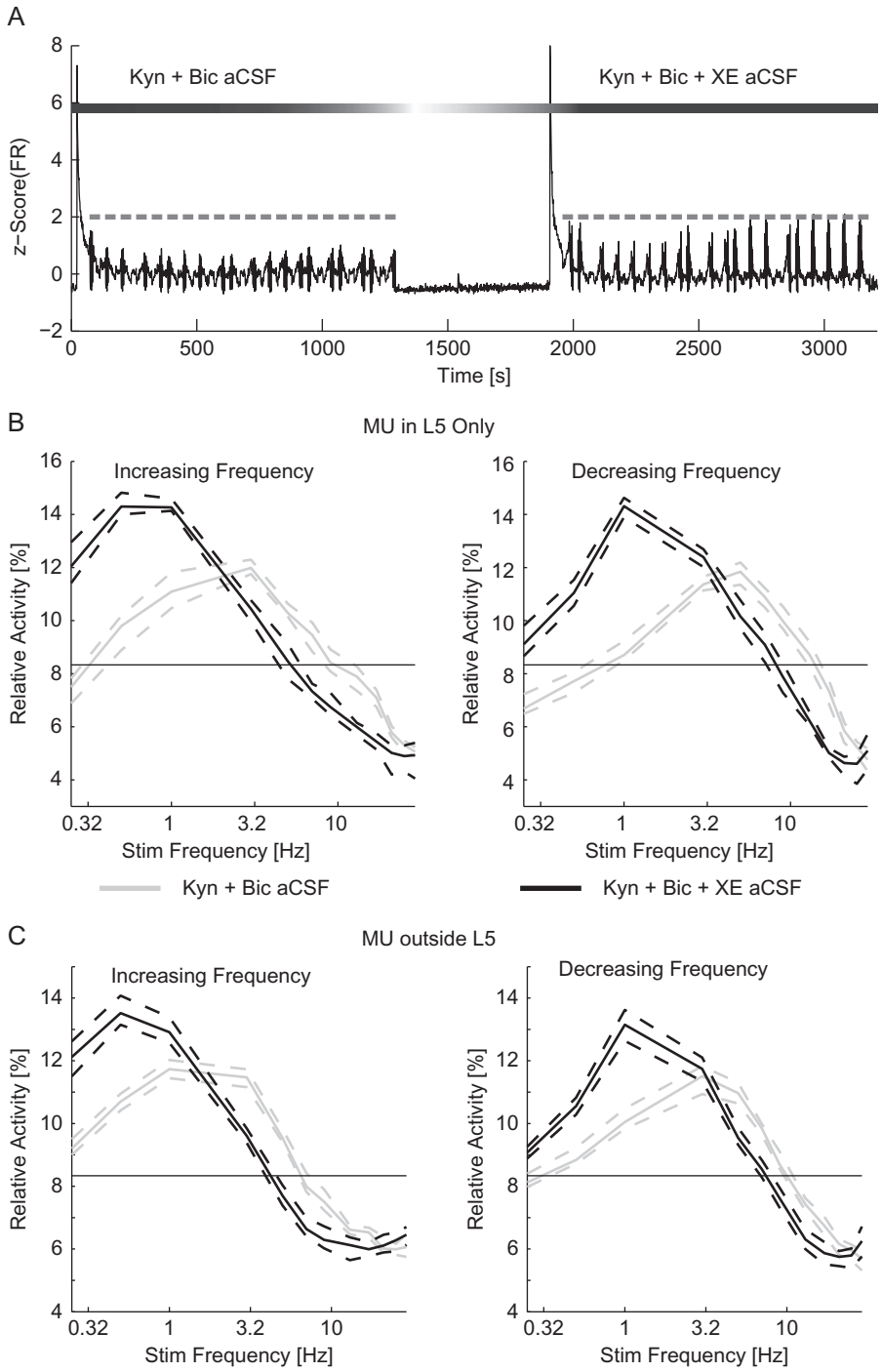

Figure 5. XE-991 remained effective in the presence of suppressed synaptic transmission. (*A*) The z-scored time course of the MU firing rate (black). Optogenetic chirp trials are indicated in gray. Synaptic transmission was suppressed throughout the experiment, after the first epoch of trials the perfusion was switched to Kyn + Bic + XE aCSF. Ten minutes after the application of Kyn + Bic + XE aCSF, a second epoch of optogenetic chirp stimulation was applied to examine the effect of I_M when synaptic transmission was suppressed. (*B*) The relative activity for each frequency of stimulation for increasing (left) and decreasing (right) frequency chirps for MU within L5. (*C*) The relative activity for MU outside of L5. The blockade of I_M had a significant effect on the relative activity with synaptic transmission suppressed. Dashed lines indicate the 95% confidence interval of the median.

responsive to middle frequency stimuli (n = 90 trials, 5–13 Hz for increasing frequency chirps and 7–17 Hz for decreasing frequency chirps, four-way ANOVA, Supplementary Tables 1 and 2, Fig. 6*B*). However, the MU in L5 also exhibited an increased response to low-frequency stimuli (0.25–1 Hz for increasing and decreasing frequency chirps). This result indicates that by blocking I_h the response of the network was shifted to favor lower frequencies. MU outside of L5 also exhibited an increase response to low-frequency stimulation (increased response to 0.25 and 0.5 Hz stimuli regardless of chirp direction and decreased response to 5–9 Hz for increasing frequency chirps and 9–13 Hz for decreasing frequency chirps, four-way ANOVA,

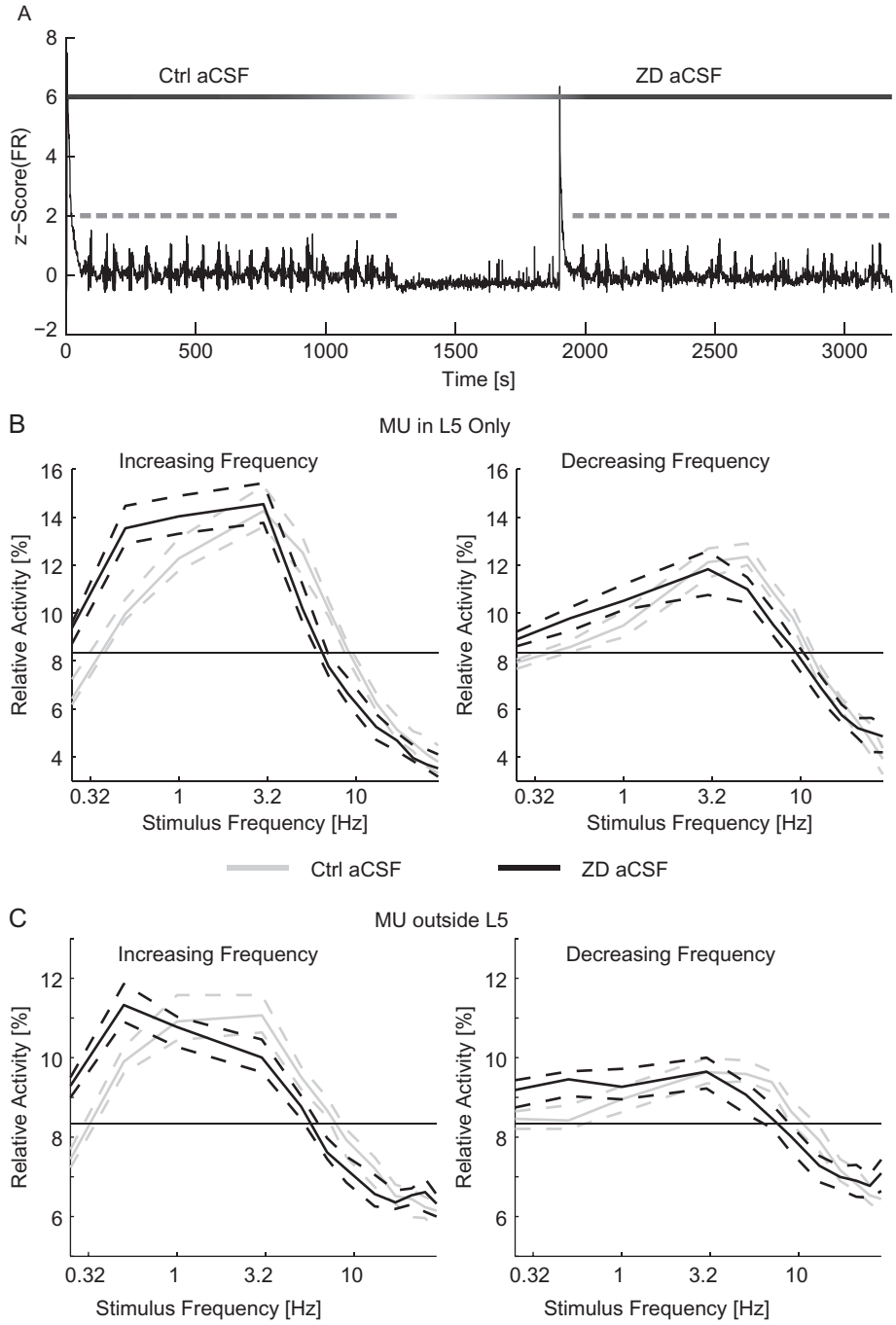

Figure 6. Blockade of I_h reduced the resonant frequency of networks. (*A*) The z-scored time course of the MU firing rate for the duration of an experiment (black). Optogenetic chirps are indicated in gray. After the first epoch of stimulation with control aCSF the perfusion was switched to ZD aCSF. Ten minutes after the addition of ZD-7288, a second epoch of stimulation was applied. The relative activity of MU recorded in L5 (*B*) and MU recorded outside of L5 (*C*) for increasing (left) and decreasing (right) frequency stimuli. For chirps in control aCSF (gray) and ZD aCSF (black). The thin black line indicates chance activity levels. With ZD-7288 in the bath, the responses to low-frequency stimuli were increased. Ctrl aCSF, control aCSF. Dashed lines indicate the 95% confidence interval of the median.

Supplementary Tables 3 and 4, Fig. 6*C*). With I_h blocked, the resonant frequency of the network shifted toward lower frequencies (increasing frequency sweeps: 2.84 [2.71–3.00] Hz for control aCSF and 1.91 [1.64–2.18] Hz for ZD aCSF, decreasing frequency sweeps: 4.54 [4.31–4.82] Hz for control aCSF and 3.04 [2.56–3.83] Hz for ZD aCSF, $P = 0.005$ for increasing frequency sweeps and $P < 10^{-3}$ for decreasing frequency sweeps ANOVA, $n = 90$ trials for each condition). This result indicates that the change in the response of L5 cells propagated throughout the network to reduce the resonant frequency of the network.

We next considered how I_h interacts with synaptic transmission to contribute to the frequency response at the network scale. To separate these 2 components, we performed experiments with both excitatory and inhibitory synaptic transmission suppressed for the duration of the experiment and examined the effect of blocking I_h in addition. The addition of

ZD-7288 to Kyn + Bic aCSF during the second epoch of trials (after a first epoch using Kyn + Bic aCSF) allowed us to assess the effect of I_h on the frequency response of the network in isolation (Fig. 7A, time course of a typical experiment). Further blocking, I_h did not significantly reduce the response to the conditioning stimulus for MU inside or outside of L5 (MU in L5: 2.69 [2.55–3.04] spikes/s in Kyn + Bic aCSF and 2.93 [2.60–3.19] spikes/s in Kyn + Bic + ZD aCSF, MU outside of L5: 1.79 [1.67–1.90] spikes/s in Kyn + Bic aCSF and 1.76 [1.66–1.90] spikes/s in Kyn + Bic + ZD aCSF, $n = 200$ trials, $P = 0.327$ and 0.253, respectively, Wilcoxon-ranked sum). With synaptic transmission suppressed, the L5 response to the chirp stimulus was only different for 0.5 Hz stimulus for increasing frequency chirps and 1 Hz for decreasing frequency chirps ($n = 100$ trials, $P = 0.003$ for 0.5 Hz for increasing frequency chirps, $P = 0.0164$ for 1 Hz for decreasing frequency chirps, and $P > 0.05$ otherwise, four-way ANOVA, Supplementary Tables 1 and 2, Fig. 7B). Outside of L5, there were no significant effects of blocking I_h after suppressing synaptic transmission ($n = 100$ trials, $P > 0.05$, four-way ANOVA, Supplementary Tables 3 and 4, Fig. 7C). We next examined the effect of further blocking I_h on the resonant frequency of the network with synaptic transmission suppressed. With synaptic transmission suppressed, the addition ZD to the aCSF did not significantly modulate the resonant frequency (increasing frequency sweeps: 2.12 [1.85–2.50] Hz for Kyn + Bic aCSF and 1.57 [1.34–1.75] Hz for Kyn + Bic + ZD aCSF, decreasing frequency sweeps: 3.94 [3.48–4.48] Hz for Kyn + Bic aCSF and 3.34 [3.06–3.64] Hz for Kyn + Bic + ZD aCSF, $P = 0.193$ for increasing frequency sweeps and $P = 0.110$ for decreasing frequency sweeps ANOVA, $n = 100$ trials for each condition). Therefore, the effect of the addition of ZD-7288, once synaptic transmission has been suppressed, was very limited. This result indicates that the effect of I_h was largely dependent on network activity.

We next directly compared the effect of blocking I_h in a slice with synaptic transmission intact to that of blocking I_h after synaptic transmission had been suppressed. To do so, we calculated the absolute change in relative activity caused by blocking I_h with synaptic transmission intact and with synaptic transmission suppressed. Across the entire network, the absolute change in activity levels caused by blocking I_h was greater when the network was intact (21.0 [18.5–22.7]% across all MU for blockade of I_h alone and 11.9 [11.0–12.5]% across all MU for blockade of I_h with synaptic transmission suppressed for increasing frequency chirps and 18.1 [16.9–21.1]% across all MU for blockade of I_h alone and 11.7 [10.4–12.8]% across all MU for blockade of I_h with synaptic transmission suppressed for decreasing frequency chirps, $n = 90$ pairs of trials for synaptic transmission intact and 100 pairs of trials for suppressed synaptic transmission, $P < 10^{-3}$ for both increasing and decreasing frequency chirps separately by Wilcoxon-ranked sum, Fig. 8A). Specifically, the increase in response to low-frequency stimulation (0.25–1 Hz for both increasing and decreasing frequency chirps) and the decrease in response to middle frequency band (5–13 Hz for increasing frequency chirps and 9–13 Hz for decreasing frequency chirps) stimulation was greater with synaptic transmission intact ($P < 0.05$, three-way ANOVA, Fig. 8B). The effect of blocking I_h was larger with synaptic transmission intact. We interpret these results to indicate that the main effect of I_h on network resonance was dependent on synaptic transmission.

Discussion

Oscillations cause time windows during which neuronal interaction is facilitated by synchronized depolarization of the membrane voltage (Steriade et al. 1993); such a mechanism enables the emergence of dynamic cell assemblies that serve as the building blocks of neuronal processing (Harris et al. 2003; Womelsdorf et al. 2014). Emerging large-scale organization of neuronal firing directly correlates with cognition and behavior and therefore is a likely candidate for the mechanism that bridges brain activity and behavior (Wang 2010). Therefore, understanding the causal mechanisms by which cortical oscillations are recruited will offer insights into how cellular and synaptic properties interact to enable information processing in cortex. Here we have examined suprathreshold resonance of networks. In this approach the MU are oscillators which are coupled by synaptic transmission. This metric of resonance is different from those used for subthreshold oscillations. Subthreshold resonance measures the frequency response of membrane impedance of single cells in isolation as an indicator of how these cells may contribute to oscillations. Here we show that I_M and I_h contribute to suprathreshold resonance on the scale of networks.

Optogenetic stimulation of networks with cell-type specificity offers the opportunity for causal interrogation of circuit dynamics (Scanziani and Hausser 2009; Cho et al. 2015). Here we have utilized multielectrode array recordings of acute cortical slices to study the intrinsic and synaptic mechanisms of network resonance by suprathreshold optogenetic stimulation of L5 PYs. The cortical networks exhibited a frequency preference for delta and theta band stimulation of L5 PYs. Blockade of KCNQ or HCN channels boosted the response to low-frequency stimuli. We further examined the interaction of I_M and I_h with synaptic transmission. The blockade of KCNQ channels caused an increased response for low-frequency stimuli regardless of the state of synaptic transmission. Conversely, when synaptic transmission was suppressed, there was a minimal effect of blocking HCN channels. These results suggest that KCNQ and HCN channels play differential roles in resonance of networks based on the dependency of the effect on synaptic transmission. Interestingly, the blockade of I_h, I_M, or suppression of synaptic transmission did not fully remove resonance from the network. These manipulations reduced the resonant frequency of the network, but did not completely change the response of the network to that of a low-pass filter.

Importantly, both KCNQ and HCN channels may enable subthreshold resonance in individual neurons; in particular, the time constant of these channels mediates a suppression of slow input by effectively high-pass filtering the input. Therefore, both types of channels are ideally situated to selectively amplify oscillations in the theta frequency band (Hutcheon and Yarom 2000). Numerous studies have confirmed such resonance dynamics by application of low-amplitude (subthreshold), frequency-modulated current injection into different excitatory cell types in a range of brain structures including, most importantly for the discussion here, L5 PYs (Hutcheon et al. 1996; Fellous et al. 2001), but also hippocampus (Leung and Yu 1998; Pike et al. 2000; Hu et al. 2002), subiculum (Wang et al. 2006), and entorhinal cortex (Alonso and Llinas 1989; Dickson et al. 2000; Giocomo et al. 2007; Nolan et al. 2007). However, it remains unclear if the extrapolation from intrinsic dynamics in disconnected hyperpolarized cells to active networks holds true. In particular, I_h-dependent theta resonance was found to be absent for experimentally depolarized individual neurons in vitro (Halliwell and Adams 1982; McCormick and Pape 1990; Hu et al. 2002; Erchova et al. 2004). Yet, theta peak frequency in vivo correlates with functional organization of

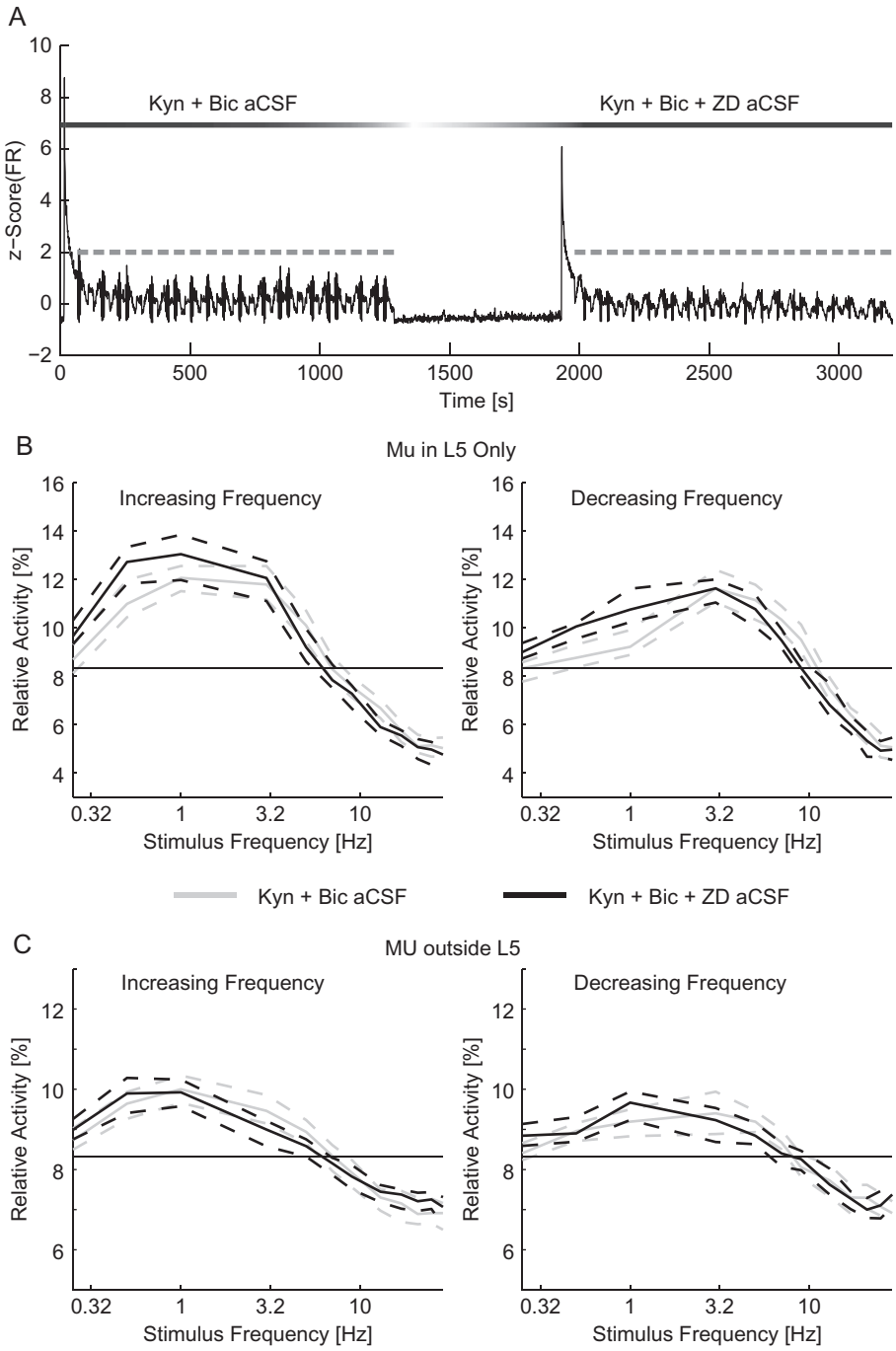

Figure 7. I_h played a limited role in resonance when synaptic transmission was suppressed. (*A*) The z-scored time course of the MU firing rate for the duration of an experiment (black). Optogenetic chirps are indicated in gray. After the first epoch of stimulation with Kyn + Bic aCSF the perfusion was switched to Kyn + Bic + ZD aCSF. Ten minutes after the addition of ZD, a second epoch of stimulation was applied. The relative activity of MU recorded in L5 (*B*) and MU recorded outside of L5 (*C*) for increasing (left) and decreasing (right) frequency stimuli. For chirps in Kyn + Bic aCSF (gray) and Kyn + Bic + ZD aCSF (black). The thin black line indicates chance activity levels. The addition of ZD-7288 caused a limited change in the frequency response, indicating that with synaptic transmission suppressed I_h played a small role in the frequency response. Dashed lines indicate the 95% confidence interval of the median.

grid cells in entorhinal cortex and with single-cell resonance peak frequencies, strongly supporting a direct link between intrinsic cellular resonance and network-level oscillations (Giocomo and Hasselmo 2009). Furthermore, cellular resonance could provide a mechanism for frequency-specific filtering of incoming synaptic input in intact networks (Izhikevich et al. 2003).

In the intact animal, mPFC networks may preferentially respond to stimuli in the high delta to low theta range from any one of the multiple types of oscillatory inputs. For example, parvalbumin positive (PV^+) interneurons can drive neocortical and hippocampal theta oscillations in vivo (Stark et al. 2013). Local optogenetic stimulation was applied to small networks of 2–20 PV^+ cells (Royer et al. 2012; Stark et al. 2012), the resulting

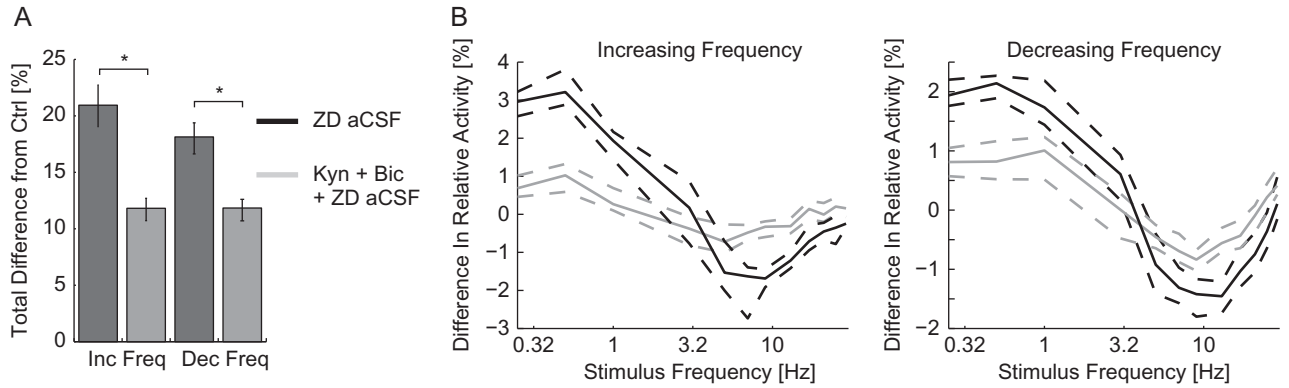

Figure 8. The effect of I_h depended on synaptic transmission. (A) The sum of the absolute difference in relative activity caused by the addition of ZD-7288 to control aCSF (dark gray) and Kyn + Bic aCSF (light gray) across frequencies. For both increasing (left) and decreasing (right) frequency chirps, the effect of adding ZD-7288 was greater without synaptic transmission suppressed. (B) The difference in relative activity by frequency across all MU for increasing (left) and decreasing (right) frequency chirps. Both the increased response to low-frequency stimuli and the decreased response in the middle frequency band were greater with synaptic transmission intact. Ctrl aCSF, control aCSF; Inc Freq, increasing frequency chirps; Dec Freq, decreasing frequency chirps. *$P < 0.05$. Dashed lines indicate the 95% confidence interval of the median. Data presented here are a direct comparison of the results of experiments presented in Figures 6 and 7.

spiking activity of the pyramidal cells exhibited theta band resonance. Furthermore with I_h blocked, the resonant profile of the excitatory cells was removed. Conversely, stimulation of all subtypes of excitatory cells (under the CaMKII promoter) resulted in a frequency response without resonance, in this case a more-or-less flat response across frequencies. Some methodological differences may explain the variation between these results and those presented here. Specifically, here we have directly stimulated only L5 PYs (under the Thy1 promoter) and have stimulated and recorded on a larger spatial scale. Stark and colleagues applied optogenetic stimulation in such a way as to record from the same cells which were directly stimulated. Conversely, here cells within layers outside of L5 did not express ChR2 in our preparation and were not directly activated by light stimulation.

Here, we have treated L5 PYs as a homogenous group; however, there exist 2 subtypes based on the axonal projections (for review: Shepherd 2013). L5 PYs, which project to the contralateral region of cortex and the striatum, the so-called intra-telencephalic cells, exhibit fewer HCN channels than those that project to other subcortical structures (Sheets et al. 2011). The magnitude of I_h is, therefore, lower in these cells (Dembrow et al. 2010; Sheets et al. 2011; Gee et al. 2012). The intra-telencephalic neurons, with lower magnitude I_h currents, exhibit a low-pass filter response without a resonant peak in the theta band (Dembrow et al. 2010). Due to differential expression of I_h and similar expression of I_M between intra-telencephalic and pyramidal tract neurons, it is likely that the lack of subthreshold resonance in intra-telencephalic L5 PYs is due to I_h (Dembrow et al. 2010). Here, we have observed subthreshold resonance in patch experiments but have not attempted to abolish it with the application of either ZD-7288 or XE-991. It is unlikely that the population that was optogenetically stimulated was dominated by either subtype of L5 PYs. The intratelencephalic neurons vary from pyramidal tract neurons in input impedance, spike threshold, and spike duration (Hattox and Nelson 2007; Dembrow et al. 2010; Suter et al. 2013). However, a previous study observed no significant difference in these metrics between L5 PYs that express ChR2 under the Thy1 promoter and those that do not (Wang et al. 2007). Additionally, in our patch experiments, we observed a variety of resonance profiles and magnitudes of I_h, as measured by the sag ratio, in the eYFP (and thus ChR2) labeled cells.

Together, our data present a novel perspective on the role of L5 PYs in propagating delta and theta band resonance of networks. Our combined pharmacological and optogenetic manipulations support a model where intrinsic excitability regulated by KCNQ and HCN channels represents a fundamental mechanism by which periodic input is translated into network-level frequency response.

Supplementary Material

Supplementary material can be found at: http://www.cercor.oxfordjournals.org/.

Funding

Research reported in this publication was supported in part by the National Institute of Mental Health of the National Institutes of Health under Award nos. (R01MH101547) and (R21MH105557–01). The content is solely the responsibility of the authors and does not necessarily represent the official views of the National Institutes of Health. A.I. was funded by the Summer Undergraduate Research Fellowship from the Office of Undergraduate Research at University of North Carolina at Chapel Hill. The UNC Neuroscience Center Microscopy Core is supported by National Institute of Neurological Disorders and Stroke Center Grant (P30 NS045892). The LCCC Animal Studies core is supported in part by National Cancer Institute Center Core Support Grant (CA16086).

Authorship Statement

S.S. and F.F. designed the experiments; S.S., C.D., and A.I. performed the experiments; S.S. analyzed the data; and S.S. and F.F. wrote the paper.

Notes

The authors thank the members of the Fröhlich lab for their valuable contributions. The authors also thank Chunxiu Yu, Joshua Jennings, and the UNC Neuroscience Center Microscopy Core (P30 NS045892) assistance with the wide field fluorescence

images. The authors also thank Alban Foulser who performed preliminary experiments and the LCCC Animal Studies Core who managed the mouse colony. *Conflict of Interest*: None declared.

References

Achermann P, Borbely AA. 1997. Low-frequency (<1 Hz) oscillations in the human sleep electroencephalogram. Neuroscience. 81:213–222.

Alonso A, Llinas RR. 1989. Subthreshold Na+-dependent theta-like rhythmicity in stellate cells of entorhinal cortex layer II. Nature. 342:175–177.

Arenkiel BR, Peca J, Davison IG, Feliciano C, Deisseroth K, Augustine GJ, Ehlers MD, Feng G. 2007. In vivo light-induced activation of neural circuitry in transgenic mice expressing channelrhodopsin-2. Neuron. 54:205–218.

Bazhenov M, Timofeev I, Steriade M, Sejnowski TJ. 2002. Model of thalamocortical slow-wave sleep oscillations and transitions to activated States. J Neurosci. 22:8691–8704.

Beltramo R, D'Urso G, Dal Maschio M, Farisello P, Bovetti S, Clovis Y, Lassi G, Tucci V, De Pietri Tonelli D, Fellin T. 2013. Layer-specific excitatory circuits differentially control recurrent network dynamics in the neocortex. Nat Neurosci. 16:227–234.

Buzsáki G. 2006.Rhythms of the brain. Oxford, New York: Oxford University Press.

Chauvette S, Volgushev M, Timofeev I. 2010. Origin of active states in local neocortical networks during slow sleep oscillation. Cereb Cortex. 20:2660–2674.

Cho KK, Hoch R, Lee AT, Patel T, Rubenstein JL, Sohal VS. 2015. Gamma rhythms link prefrontal interneuron dysfunction with cognitive inflexibility in Dlx5/6(+/–) mice. Neuron. 85:1332–1343.

Crochet S, Petersen CC. 2006. Correlating whisker behavior with membrane potential in barrel cortex of awake mice. Nat Neurosci. 9:608–610.

Cuntz H, Remme MW, Torben-Nielsen B. 2014.The computing dendrite: from structure to function. New York: Springer.

Dembrow NC, Chitwood RA, Johnston D. 2010. Projection-specific neuromodulation of medial prefrontal cortex neurons. J Neurosci. 30:16922–16937.

Dickson CT, Magistretti J, Shalinsky MH, Fransen E, Hasselmo ME, Alonso A. 2000. Properties and role of I(h) in the pacing of subthreshold oscillations in entorhinal cortex layer II neurons. J Neurophysiol. 83:2562–2579.

Engel TA, Schimansky-Geier L, Herz AV, Schreiber S, Erchova I. 2008. Subthreshold membrane-potential resonances shape spike-train patterns in the entorhinal cortex. J Neurophysiol. 100:1576–1589.

Erchova I, Kreck G, Heinemann U, Herz AV. 2004. Dynamics of rat entorhinal cortex layer II and III cells: characteristics of membrane potential resonance at rest predict oscillation properties near threshold. J Physiol. 560:89–110.

Fellous JM, Houweling AR, Modi RH, Rao RP, Tiesinga PH, Sejnowski TJ. 2001. Frequency dependence of spike timing reliability in cortical pyramidal cells and interneurons. J Neurophysiol. 85:1782–1787.

Fransen E, Alonso AA, Dickson CT, Magistretti J, Hasselmo ME. 2004. Ionic mechanisms in the generation of subthreshold oscillations and action potential clustering in entorhinal layer II stellate neurons. Hippocampus. 14:368–384.

Gee S, Ellwood I, Patel T, Luongo F, Deisseroth K, Sohal VS. 2012. Synaptic activity unmasks dopamine D2 receptor modulation of a specific class of layer V pyramidal neurons in prefrontal cortex. J Neurosci. 32:4959–4971.

Gentet LJ, Avermann M, Matyas F, Staiger JF, Petersen CC. 2010. Membrane potential dynamics of GABAergic neurons in the barrel cortex of behaving mice. Neuron. 65:422–435.

Giocomo LM, Hasselmo ME. 2009. Knock-out of HCN1 subunit flattens dorsal-ventral frequency gradient of medial entorhinal neurons in adult mice. J Neurosci. 29:7625–7630.

Giocomo LM, Zilli EA, Fransen E, Hasselmo ME. 2007. Temporal frequency of subthreshold oscillations scales with entorhinal grid cell field spacing. Science. 315:1719–1722.

Haas JS, White JA. 2002. Frequency selectivity of layer II stellate cells in the medial entorhinal cortex. J Neurophysiol. 88:2422–2429.

Halliwell JV, Adams PR. 1982. Voltage-clamp analysis of muscarinic excitation in hippocampal neurons. Brain Res. 250:71–92.

Harris KD, Csicsvari J, Hirase H, Dragoi G, Buzsaki G. 2003. Organization of cell assemblies in the hippocampus. Nature. 424:552–556.

Hattox AM, Nelson SB. 2007. Layer V neurons in mouse cortex projecting to different targets have distinct physiological properties. J Neurophysiol. 98:3330–3340.

Hu H, Vervaeke K, Storm JF. 2002. Two forms of electrical resonance at theta frequencies, generated by M-current, h-current and persistent Na+ current in rat hippocampal pyramidal cells. J Physiol. 545:783–805.

Hutcheon B, Miura RM, Puil E. 1996. Subthreshold membrane resonance in neocortical neurons. J Neurophysiol. 76:683–697.

Hutcheon B, Yarom Y. 2000. Resonance, oscillation and the intrinsic frequency preferences of neurons. Trends Neurosci. 23:216–222.

Izhikevich EM, Desai NS, Walcott EC, Hoppensteadt FC. 2003. Bursts as a unit of neural information: selective communication via resonance. Trends Neurosci. 26:161–167.

Jameson LC, Sloan TB. 2006. Using EEG to monitor anesthesia drug effects during surgery. J Clin Monit Comput. 20:445–472.

Kole MH, Hallermann S, Stuart GJ. 2006. Single Ih channels in pyramidal neuron dendrites: properties, distribution, and impact on action potential output. J Neurosci. 26:1677–1687.

Leung LS, Yu HW. 1998. Theta-frequency resonance in hippocampal CA1 neurons in vitro demonstrated by sinusoidal current injection. J Neurophysiol. 79:1592–1596.

Lorincz A, Notomi T, Tamas G, Shigemoto R, Nusser Z. 2002. Polarized and compartment-dependent distribution of HCN1 in pyramidal cell dendrites. Nat Neurosci. 5:1185–1193.

Luczak A, Bartho P, Marguet SL, Buzsaki G, Harris KD. 2007. Sequential structure of neocortical spontaneous activity in vivo. Proc Natl Acad Sci USA. 104:347–352.

Luthi A, McCormick DA. 1998. H-current: properties of a neuronal and network pacemaker. Neuron. 21:9–12.

Magee JC. 2000. Dendritic integration of excitatory synaptic input. Nat Rev Neurosci. 1:181–190.

Marshall L, Helgadottir H, Molle M, Born J. 2006. Boosting slow oscillations during sleep potentiates memory. Nature. 444:610–613.

McCormick DA, Pape HC. 1990. Properties of a hyperpolarization-activated cation current and its role in rhythmic oscillation in thalamic relay neurones. J Physiol. 431:291–318.

Mitra P, Bokil H. 2008. Observed brain dynamics. Oxford, New York: Oxford University Press.

Nolan MF, Dudman JT, Dodson PD, Santoro B. 2007. HCN1 channels control resting and active integrative properties of stellate cells from layer II of the entorhinal cortex. J Neurosci. 27:12440–12451.

Pike FG, Goddard RS, Suckling JM, Ganter P, Kasthuri N, Paulsen O. 2000. Distinct frequency preferences of different types of rat hippocampal neurones in response to oscillatory input currents. J Physiol. 529 (Pt 1):205–213.

Rotstein HG. 2015. Subthreshold amplitude and phase resonance in models of quadratic type: Nonlinear effects generated by the interplay of resonant and amplifying currents. J Comput Neurosci. 38:325–354.

Rotstein HG, Nadim F. 2014. Frequency preference in two-dimensional neural models: a linear analysis of the interaction between resonant and amplifying currents. J Comput Neurosci. 37:9–28.

Rotstein HG, Pervouchine DD, Acker CD, Gillies MJ, White JA, Buhl EH, Whittington MA, Kopell N. 2005. Slow and fast inhibition and an H-current interact to create a theta rhythm in a model of CA1 interneuron network. J Neurophysiol. 94:1509–1518.

Royer S, Zemelman BV, Losonczy A, Kim J, Chance F, Magee JC, Buzsaki G. 2012. Control of timing, rate and bursts of hippocampal place cells by dendritic and somatic inhibition. Nat Neurosci. 15:769–775.

Sanchez-Vives MV, McCormick DA. 2000. Cellular and network mechanisms of rhythmic recurrent activity in neocortex. Nat Neurosci. 3:1027–1034.

Santoro B, Chen S, Luthi A, Pavlidis P, Shumyatsky GP, Tibbs GR, Siegelbaum SA. 2000. Molecular and functional heterogeneity of hyperpolarization-activated pacemaker channels in the mouse CNS. J Neurosci. 20:5264–5275.

Scanziani M, Hausser M. 2009. Electrophysiology in the age of light. Nature. 461:930–939.

Schmidt SL, Chew EY, Bennett DV, Hammad MA, Frohlich F. 2013. Differential effects of cholinergic and noradrenergic neuromodulation on spontaneous cortical network dynamics. Neuropharmacology. 72C:259–273.

Schmidt SL, Iyengar AK, Foulser AA, Boyle MR, Frohlich F. 2014. Endogenous cortical oscillations constrain neuromodulation by weak electric fields. Brain Stimul. 7:878–889.

Sellers KK, Bennett DV, Frohlich F. 2014. Frequency-band signatures of visual responses to naturalistic input in ferret primary visual cortex during free viewing. Brain Res. 1598:31–45.

Sheets PL, Suter BA, Kiritani T, Chan CS, Surmeier DJ, Shepherd GM. 2011. Corticospinal-specific HCN expression in mouse motor cortex: I(h)-dependent synaptic integration as a candidate microcircuit mechanism involved in motor control. J Neurophysiol. 106:2216–2231.

Shepherd GM. 2013. Corticostriatal connectivity and its role in disease. Nat Rev Neurosci. 14:278–291.

Stark E, Eichler R, Roux L, Fujisawa S, Rotstein HG, Buzsaki G. 2013. Inhibition-induced theta resonance in cortical circuits. Neuron. 80:1263–1276.

Stark E, Koos T, Buzsaki G. 2012. Diode probes for spatiotemporal optical control of multiple neurons in freely moving animals. J Neurophysiol. 108:349–363.

Steriade M, Nunez A, Amzica F. 1993. Intracellular analysis of relations between the slow (<1 Hz) neocortical oscillation and other sleep rhythms of the electroencephalogram. J Neurosci. 13:3266–3283.

Steriade M, Timofeev I, Grenier F. 2001. Natural waking and sleep states: a view from inside neocortical neurons. J Neurophysiol. 85:1969–1985.

Suter BA, Migliore M, Shepherd GM. 2013. Intrinsic electrophysiology of mouse corticospinal neurons: a class-specific triad of spike-related properties. Cereb Cortex. 23:1965–1977.

Tononi G, Cirelli C. 2014. Sleep and the price of plasticity: from synaptic and cellular homeostasis to memory consolidation and integration. Neuron. 81:12–34.

Ulrich D. 2002. Dendritic resonance in rat neocortical pyramidal cells. J Neurophysiol. 87:2753–2759.

Wang H, Peca J, Matsuzaki M, Matsuzaki K, Noguchi J, Qiu L, Wang D, Zhang F, Boyden E, Deisseroth K, et al. 2007. High-speed mapping of synaptic connectivity using photostimulation in Channelrhodopsin-2 transgenic mice. Proc Natl Acad Sci USA. 104:8143–8148.

Wang WT, Wan YH, Zhu JL, Lei GS, Wang YY, Zhang P, Hu SJ. 2006. Theta-frequency membrane resonance and its ionic mechanisms in rat subicular pyramidal neurons. Neuroscience. 140:45–55.

Wang XJ. 2010. Neurophysiological and computational principles of cortical rhythms in cognition. Physiol Rev. 90:1195–1268.

Womelsdorf T, Valiante TA, Sahin NT, Miller KJ, Tiesinga P. 2014. Dynamic circuit motifs underlying rhythmic gain control, gating and integration. Nat Neurosci. 17:1031–1039.

Yoshida M, Giocomo LM, Boardman I, Hasselmo ME. 2011. Frequency of subthreshold oscillations at different membrane potential voltages in neurons at different anatomical positions on the dorsoventral axis in the rat medial entorhinal cortex. J Neurosci. 31:12683–12694.

Zhuchkova E, Remme MW, Schreiber S. 2013. Somatic versus dendritic resonance: differential filtering of inputs through non-uniform distributions of active conductances. PLoS One. 8:e78908.